Inflow and shock formation in supersonic, rarefied plasma expansions

Inflow and shock formation in supersonic, rarefied plasma expansions

P. Vankan
Department of Applied Physics, Eindhoven University of Technology, P.O. Box 513, 5600 MB Eindhoven, The Netherlands

S. Mazouffre
Laboratoire d'Aerothermique, 1C Avenue de la Recherche Scientifique, 45071 Orleans, France

R. Engeln[a] and D. C. Schram
Department of Applied Physics, Eindhoven University of Technology, P.O. Box 513, 5600 MB Eindhoven, The Netherlands

(Received 26 April 2005; accepted 30 August 2005; published online 6 October 2005)

In this paper the physics of plasma expansion in the rarefied regime is reviewed. Densities, temperatures, and velocity distributions in argon, hydrogen, and nitrogen expansions that have been measured using laser scattering and fluorescence techniques are compared. The velocity distributions in the region of the expansion where the density is below the background density show a bimodal character. It is interpreted in terms of a component expanding from the source and a component flowing into the plasma expansion from the periphery. Also in the shock of the expansion, bimodal velocity distributions are encountered. These distributions show the gradual change in the flow from supersonic to subsonic—the formation of the shock. From a comparison of the three expansions, a general view of the shock formation is derived. This new insight leads to a better understanding of how the chemical reactivity of the usually impenetrable, supersonic plasma can be used most efficiently. © *2005 American Institute of Physics*. [DOI: 10.1063/1.2076507]

I. INTRODUCTION

Supersonic expansions occur between regions with sufficient pressure difference. In plasmas, an expansion is therefore a logical consequence. Plasma is created by applying a large power density to a limited volume. Therefore, the temperature rises and the pressure increases. As a consequence the plasma will expand from the source region to the lower-pressure background region, unless restrained by, e.g., walls or electric/magnetic forces. If the power density in the source region is high and the pressure in the background is low, the pressure may vary over many orders of magnitude, and a supersonic expansion is formed. A thorough understanding of the plasma-expansion properties is crucial in fields such as astrophysics,[1] high-rate deposition,[2–4] and surface modification.[5]

In expansions, both plasma and gaseous, the mixing of the expansion with its background is of key importance in a number of applications such as hypersonic propulsion, chemical lasers, plasma deposition, and plasma spraying.[2,4,6] In, for example, jet engines, such as scramjets and air-breathing jet engines,[6,7] the mixing of the fuel with air or oxygen in the supersonic flows is of key importance for an efficient combustion. In all the mentioned applications supersonic flows are used, which greatly limits the mixing process. Whereas a subsonic flow mixes well with the background gas, a supersonic flow is a closed structure, which is not easily penetrated. In other words, for supersonic expansions, the mixing zone is thin, especially at the relatively high pressures encountered in most applications. Mixing is then usually enhanced by a number of techniques such as nozzle design and turbulent mixing.[7] When the densities are lower, the mixing zone becomes broader, and at low enough densities, i.e., in the rarefied regime, mixing with the background may even become a natural phenomenon. We here present measurements that show the mixing of a plasma expansion with the background gas in the rarefied regime.

The plasma expansion under investigation is used for high-rate deposition of thin films. In this research area, a method that is encountered more and more is the remote source technique. The plasma source and treatment region are in this technique separated and can, therefore, both be optimized individually. The primary reactive particles are transported from the source to the treatment region via a supersonic expansion. The deposition precursors are produced during the transport from precursor gases that are injected into the periphery of the expansion. It is evident that the properties of the expansion as well as the admixture of the injected precursor gases into the primary plasma beam is of relevance. Two examples can be found in the deposition of diamond-like carbon films and amorphous and nanocrystalline silicon layers.[2,4] In the first application, C_2H_2 molecules admix into the plasma beam upon injection into the periphery of the expansion. In the plasma beam they undergo a series of reactions to create those radicals that are of primary importance for the deposition of diamond-like carbon films.[2,8–10] In the second example, SiH_4 molecules admix into the plasma. Through collisions, in this case with hydrogen atoms, the hydrogen atom is stripped from the silane molecules, forming a SiH_3 radical. These radicals play a dominant role in the deposition of amorphous and nanocrystalline silicon films.[11,12]

[a]Author to whom correspondence should be addressed. Electronic mail: r.engeln@phys.tue.nl

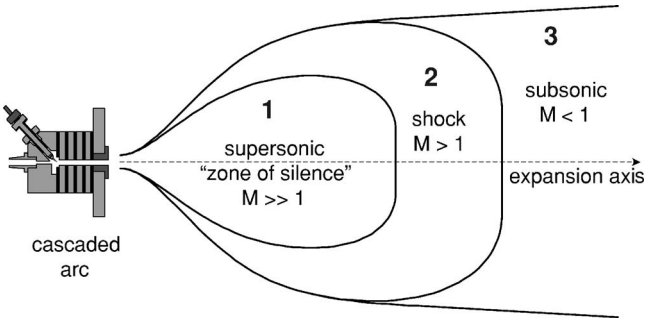

FIG. 1. Schematic representation of the source and the plasma expansion.

It is evident that an efficient admixing of deposition precursor gases into the plasma beam is important to efficiently use the reactivity produced in the source. However, admixing into the supersonic plasma is usually difficult due to the high viscosity of plasma and due to the high velocities. In the rarefied regime conditions are reached that enhance efficient admixing of injected precursor gases, due to the low density, to long collisional mean free paths. We will show that in the rarefied regime atoms or molecules can already enter the plasma in the supersonic regime of the expansion. This inflow can occur because the mean free path is in the order of the radial size of the expansion. Naturally, mixing also occurs in the subsonic part of the expansion, via diffusion of the background gas into the expansion.

The collisions of the entering particles with the particles in the plasma expansion firstly promote the reactions of the secondary chemistry, i.e., the actual creation of, e.g., the deposition precursors. Secondly, they have influence on the shock formation in the rarefied regime. In the shock, the flow changes from supersonic to subsonic in a highly nonequilibrium way.[13–15] This is, for example, reflected in the velocity distribution function (vdf). The vdf behavior in the shock wave gives more insight in the phenomenon of shock formation.

In this paper, we will first describe the general properties of rarefied plasma expansion. Next, the experiments will be described and some measurements that may show the inflow into the plasma expansion will be discussed. Finally, we will discuss measured velocity distribution functions in the shocks of argon, hydrogen, and nitrogen expansions that reveal the characteristic shock formation in those expansions.

II. RAREFIED PLASMA EXPANSION

In Fig. 1, the plasma source and the plasma expansion are depicted schematically. In the plasmas that are discussed in this paper, the ionization degree is 10% or even much less. The plasma expansion is then almost like that of a hot gas:[16–20] while expanding from the source, it accelerates and both the temperature and the density decrease. When the jet total pressure[21] approaches the background pressure, the flow goes through a stationary shock, after which the plasma expands subsonically.

However, there are significant differences in detail between a plasma and a gas expansion. In the plasma source the temperature at the axis is about 1 eV. The plasma source is connected to a vacuum vessel via a constant diameter nozzle. In this nozzle the temperature drops to around 0.8 eV in the case of argon and nitrogen plasmas, and to 0.25 eV in the case of a hydrogen plasma. Moreover, there are strong indications that in the source the product of density n and flow velocity w is approximately constant over the source radius,[22] whereas in a gas flow the nw product is parabolic. As a consequence, the density at the exit of the arc source can be given with reasonable accuracy by

$$n_0 = \frac{\Phi \zeta_{\mathrm{geom}}}{c_0 \pi r_o^2} \text{ with } c_0 = \sqrt{\frac{\gamma k T_s}{M}}, \tag{1}$$

in which r_0 is the radius of the arc source at the exit, Φ is the initial gas flow including ionization and dissociation, and c_0 is the frozen sound velocity in the nozzle, with γ the adiabatic coefficient, M the effective mass of plasma flow, and T_s the source temperature. ζ_{geom} is a geometrical factor that takes into account that nw may not be completely constant over the source radius. As will be shown later, $\zeta=1$ fits the argon expansion very well.

In the supersonic expansion part, we use a slightly modified formula for the axial dependence (z) of the density compared to Ashkenas and Sherman[16] and Miller[23] to make the description also valid in the source:[20]

$$n(z) = \frac{n_0 z_0^2}{z^2 + z_0^2}. \tag{2}$$

For a straight nozzle, $z_0 \simeq r_0$. The expression proves to give a good description of the measured z dependence of the supersonic expansion from a straight nozzle, as is shown in Sec. IV. It may still be valid for other, e.g., Campargue-like, nozzles, but that would require a redefinition of z_0. In the nozzle, the plasma is already flowing and at the exit the velocity is sonic (c_0). Under the assumption of an adiabatic expansion and ignoring viscosity, we can now obtain the following estimate for the axial dependence of the velocity:[24]

$$w(z) = w_\infty \sqrt{1 - \frac{2}{\gamma+1}\left(\frac{n(z)}{n_0}\right)^{\gamma-1}}. \tag{3}$$

The gas is accelerated in the supersonic expansion from the sonic speed at the exit of the nozzle until it reaches the final velocity w_∞, which is given by

$$w_\infty = c_0 \sqrt{\frac{\gamma+1}{\gamma-1}} = 2c_0 \quad \text{for } \gamma = 5/3. \tag{4}$$

Note that $\gamma=5/3$ is a good approximation, even for molecular plasmas containing molecules, atoms, ions, and electrons, since during the expansion the vibrational and rotational degrees of freedom are frozen in the expansion,[25] certainly in the case of hydrogen and to a lesser extent also for nitrogen.

In the stationary shock the density increases as a result of the decreasing velocity, ensuring continuity of the flow. With decreasing background density, the shock becomes broader with the increasing mean free path.[13] The result is a more gradual transition from the over-expanded region to the subsonic region. The end of the stationary shock is located at the position z_M. It is advantageous to rewrite the well-known

relation for z_M (Refs. 16 and 26) in terms of flow, source temperature, and background pressure, in which case the source diameter d is eliminated:

$$z_M = 0.67d\sqrt{\frac{p_0}{p_b}} = 1.8\times 10^{-2}\sqrt{\frac{\hat{\Phi}}{p_b}}\sqrt[4]{A\hat{T}_s}, \tag{5}$$

in which $\hat{\Phi}$ is the flow in scc/s (1 scc/s is equivalent to 2.5×10^{19} s^{-1}), p_b is the background pressure in Pa, A is the atomic mass number, and $\hat{T}_s$ is the source temperature at the axis in eV.

In systems like rarefied plasma expansion where the collisional mean free path of the particles is of the same order of magnitude as the system itself, one should consider the Knudsen number,

$$Kn = \frac{\lambda_{\mathrm{mfp}}}{L} \simeq \frac{w}{n\sigma v_{\mathrm{rel}} L}, \tag{6}$$

where λ_{mfp} is the collisional mean free path, w is the velocity, v_{rel} is the relative collision velocity, L is the typical size of the system, and σ is the collision cross section for momentum transfer. In the case of a rarefied plasma expansion, where atoms and molecules can enter the expansion structure, a good choice for L may be the local radius of the plasma. In the nozzle this results in $Kn \approx 0.05-0.2$. Into the supersonic expansion, the Knudsen number increases and after a few millimeters from the source the increase is proportional to z ($n \propto 1/z^2$ and $L \propto z$). In the region where the density in the expansion is lower than the density in the background gas, which we call the valley of the expansion, the Knudsen number is highest, $Kn \approx 0.2-1$. In effect, this means that an atom or molecule, which resides in the periphery of the expansion, may move into the expansion structure, even as far as the expansion axis ($Kn \approx 1$), before colliding. In other words, the expansion structure has become semitransparant. In the shock of the expansion the Knudsen number decreases again due to the increasing density and reaches values of $Kn \approx 0.05-0.2$ at the end of the shock. Finally, in the subsonic region of the expansion, the Knudsen number decreases further with increasing density.

III. EXPERIMENT

A. Plasma expansion

The plasma is generated using a cascaded arc source, which has the advantage of operation at high pressure, high power, and small volume, leading to a high-power density in the plasma. The arc channel with a diameter of 4 mm and a length of 50 mm is formed by the central holes in four insulated cascade plates. A current of 40-60 A generates a thermal plasma in flowing gas. Three different gases have been used to create a plasma expansion: argon, hydrogen, and nitrogen. In argon, a flow of 50 scc/s (standard cubic centimeter per second) and a current of 40 A is used, leading to a pressure in the arc of around 6.2×10^4 Pa.[27] In hydrogen, a flow of H_2 of 50 scc/s is used and a current of 60 A is applied, leading to a pressure of around 1.2×10^4 Pa in the arc.[28] In nitrogen, a diameter of the arc channel of 3 mm instead of 4 mm was used and a current of 55 A. Using a N_2 flow of 25 scc/s resulted in a pressure of around 4.4×10^4 Pa.[29] In all cases, the cascaded arc is connected via a nozzle to a vacuum vessel. The nozzle has a constant diameter equal to the arc channel diameter. The vacuum vessel is kept at a constant pressure between 20 and 100 Pa. Due to the large pressure difference the plasma expands supersonically into the vacuum vessel. A schematic representation of the expansion is given in Fig. 1. Since the plasma is flowing, the pressure in the nozzle has already decreased compared to the pressure in the arc.

In argon, the ionization degree of the plasma is high, typically 10%. In molecular plasmas, the situation is more complex, due to molecular processes. In the hydrogen case, there is an ionizing central plasma channel with a 1 mm radius and a weakly-ionized, partly molecular, recombining plasma at the outside. As a result the total ionization degree is smaller than 2%. In nitrogen, a comparable configuration of a central ionizing plasma with a surrounding, recombining molecular plasma is present, but the surrounding plasma is smaller in dimension and thus, the effective total ionization degree is higher (5%).

The dissociation degree in the arc channel is expected to be high, but it is strongly reduced in the nozzle by surface association. In hydrogen, the dissociation degree drops below 10% for the conditions described here, see Refs. 30 and 31. In nitrogen, the dissociation degree is higher due to the less efficient surface association.

In the nozzle and in the expansion, the ionization degree in argon remains high since the three-particle recombination is slow.[32] However, in hydrogen the recombination is stronger due to a sequence of charge transfer of atomic to molecular ions and subsequent dissociative recombination.[33] As a consequence, after a few millimeters almost no hydrogen ions are left, whereas in argon still a few percent ion fraction remains present. However, this fraction has only little influence on the expansion and we will thus consider the expansion as that of a neutral gas.[19,20] In fact, in the Ar fluorescence experiments a few percent of H_2 has been admixed to lower the ionization degree and thus the Ar^* metastable density to avoid saturation.[27] In the nitrogen plasma the recombination via molecular processes is less efficient.[29,34] Hence the ions survive longer and the ionization degree remains relatively high.

B. Laser spectroscopy

Three different laser spectroscopic techniques have been applied to the expanding plasmas. In the argon plasma, a diode laser-induced fluorescence (LIF) technique has been employed to obtain the velocity distribution functions (vdf), temperatures, and density ratios (if two distributions can be identified). An intensity-modulated external cavity diode laser is used to excite Ar^* via either the $1s_5 \rightarrow 1p_9$ (811.53 nm) or the $1s_4 \rightarrow 2p_7$ (810.37 nm) transition. The LIF signal is detected under 90° using a photomultiplier and is analyzed using a lock-in amplifier. The wavelength scale of the diode laser is calibrated by the simultaneous recording of the absorption in an argon lamp and the interference signal from a

Fabry-Pérot etalon. From a spectral scan, the vdf and temperature can now be determined. Further details can be found in Ref. 26.

Hydrogen and nitrogen atoms are probed using the two-photon absorption laser-induced fluorescence technique (TALIF).[29,35] A Nd:YAG (yttrium aluminum garnet) laser pumped dye laser is operated at a wavelength of around 615 nm for hydrogen and 621 nm for nitrogen. The laser beam is frequency-tripled using a potassium dihydrogen phosphate (KDP) and a beta-barium borate (BBO) crystal, resulting in tunable, 8 ns pulses at a wavelength of around 205 or 207 nm. The 205 nm photons are used to excite H atoms from the $1s^2S$ ground state to the $3d^2D$ and $3s^2S$ excited states via a two-photon transition. The 207 nm photons are used to excite N atoms from the $2p^4S_{3/2}$ ground state to the $3p^4S_{3/2}$ excited state, also via a two-photon transition. The resulting fluorescence at 656 nm for H atoms and at 742–747 nm for N atoms is detected by a photomultiplier tube. From a spectral scan over the two-photon transition, the H atom density, temperature, and vdf along the laser beam are obtained. In all of the measurements, the dye laser wavelength is calibrated by the simultaneous recording of the well-known absorption spectrum of molecular iodine. The measurements are furthermore corrected for all of the experimental parameters (laser power, optical transmission, detector efficiency), the linearity is checked, and the densities are calibrated using a two-photon transition in a known amount of krypton.[35]

Finally, Rayleigh scattering is used to measure the neutral densities of both argon atoms and hydrogen molecules.[15,27] The Rayleigh scattering is performed using a 230 nm laser beam, of which the details are given in Ref. 36. The scattered signal is imaged onto a gated solar-blind photomultiplier and a slit mask defines the detection volume. Absolute densities are obtained by a calibration using a known amount of argon or hydrogen.

For the LIF and TALIF measurements two directions of the incident beam have been used: one with the laser-beam incident perpendicular to the expansion and one with the laser beam incident counterpropagating to the expansion. Hence information on both perpendicular and parallel components of the vdf could be obtained. By moving the arc source in the perpendicular and parallel directions with a fixed optical system, spatial profiles can be recorded with a resolution of less than 1 mm.

IV. INFLOW

In Fig. 2, the axial profile of the argon density in an argon plasma expansion is shown. The density close to the source can indeed be derived from the flow using Eq. (1), as indicated in the figure. In the expansion, the density starts decreasing following the predicted $1/z^2$ dependence, after $z=z_0=r_0$. The density dependence can be satisfactorily described by expression (2), as indicated by the dashed line in Fig. 2. The shock position z_M (45 and 75 mm) approximately follows the values predicted by Eq. (5) for both pressures. This position is easily identified in the velocity profile, since at that position the mean jet velocity equals the velocity of sound. But, it is also visible in the density profile (Fig. 2) as the end of the abrupt increase in density.

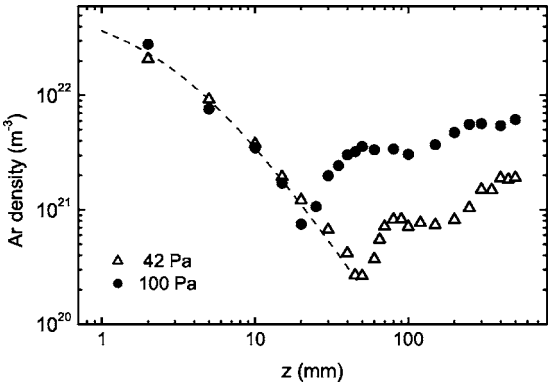

FIG. 2. Argon density profile along the jet axis of an expanding argon plasma at background pressures of 42 and 100 Pa. The dashed line represents the density dependence predicted by expression (2). The flow was 50 scc/s.

A feature that is further important in these rarefied expansions is the "valley" of the expansion, i.e., the region where the density is below the background density. In Fig. 2 the start, z_b, and end position, z_M, of the valley for $P=42$ Pa and $P=100$ Pa are 25 and 75 mm and 11 and 45 mm, respectively. In Fig. 3 z_b and z_M for $P=20$ Pa and $P=100$ Pa are 7 and 38 mm and 3 and 12 mm, respectively. Especially at the lower pressure of 42 Pa the shock valley is relatively large: $0.75z_M$. At this pressure the density in the valley is 2×10^{20} m^{-3} and the mean free path $(1/n\sigma)$ is thus about 50 mm. As this is close to the dimensions of the valley, also about 50 mm, the Knudsen number Kn becomes close to unity, making the transition from supersonic to subsonic very gradual.

In the hydrogen case, the majority particle H_2 shows a behavior, which is comparable to that of argon, as shown in Fig. 3. The density near the exit can be approximated rather well by Eq. (1). At a background pressure of 20 Pa, the expansion does follow the $1/z^2$ dependence, but in the 100 Pa case the shock position is too close to the source exit to reach the $1/z^2$ dependence. The position of the end of the shock (12 and 38 mm for the two pressures) also follows the

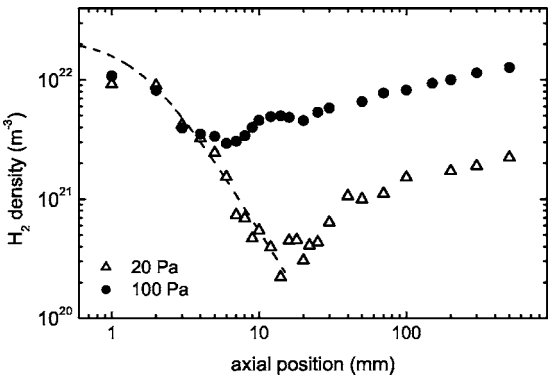

FIG. 3. Hydrogen density profile along the jet axis of an expanding hydrogen plasma at background pressures of 20 and 100 Pa. The dashed line represents the density dependence predicted by expression (2). The flow was 50 scc/s.

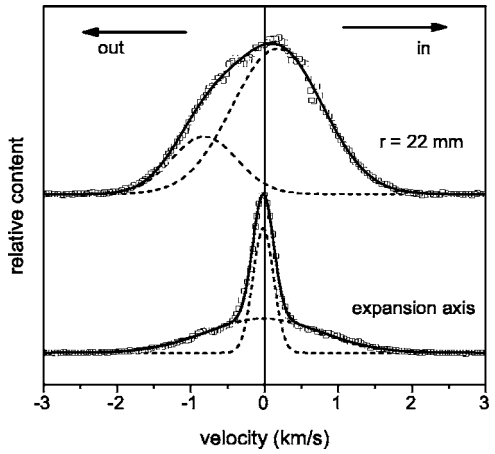

FIG. 4. Radial velocity distribution functions of argon at the center axis of the expansion ($r=0$ mm) and at a radial position of $r=22$ mm, at an axial position of $z=50$ mm. These positions are in the valley of the expansion, before the shock. The lines are the fits to the experimental data in the bimodal approximation. The background pressure was 20 Pa, which results in $z_M \approx 100$ mm.

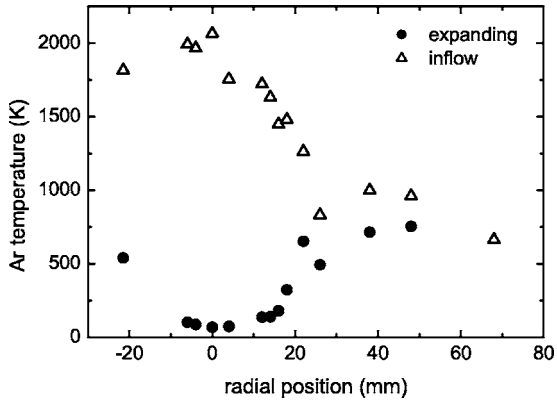

FIG. 5. Radial temperature profile at an axial position of $z=50$ mm for the two components of the bimodal approximation that is used to describe the non-Maxwellian vdfs in the valley of the argon expansion.

values predicted by Eq. (5), with the minor remark that in the 20 Pa case the predicted value is 15% lower than observed. Again the shock valley is rather long, $0.8z_M$ in the 20 Pa case, meaning that the transition from supersonic to subsonic is gradual and the expansion becomes semitransparant.

The most important consequence of a semitransparant expansion is that atoms and molecules from the periphery of the expansion can enter the valley of the expansion and can be mixed with the jet. Evidence for this effect can be found in the velocity distributions. It can, for example, be seen in Fig. 4, where two radial vdfs are shown, measured at $z=50$ mm, i.e., in the valley of the expansion, one at the expansion axis and one at $r=22$ mm. As expected the mean velocity, i.e., the first moment of the vdf, at the expansion axis is zero. However, at $r=22$ mm the mean velocity is 40 m/s in the outward direction. This velocity is smaller than the measurement accuracy, even though a much larger velocity in the outward direction is expected in an adiabatic expansion. Furthermore, both vdfs are clearly nonthermal and cannot be described by a single Maxwellian flow. But both vdfs *can* be satisfactorily described by a bimodal approximation.[13] In such a bimodal approximation, the flow is approximated by two individual Maxwellian flows, of which the separate vdfs add up to the observed vdf. A possible explanation for the radial vdfs is as follows. For the supersonic expansion region one expects particles moving in the outward radial direction, according to the corresponding expansion angle. In Fig. 4, indeed a group of such particles can be seen. It is one of the two vdf components apparent in this figure. At the center, it is the cold component with naturally zero average radial velocity. At $r=22$ mm, it is the component moving at a radial velocity of 810 m/s. At the expansion angle of 24°, one would expect a radial velocity component of around 1000 m/s, so the measured velocity is somewhat lower than expected.

Apart from the expanding component, one also observes another component. At $r=22$ mm this component of the vdf has a radial velocity in the inward direction, moving towards the expansion axis. The radial temperature profile of the two components, shown in Fig. 5, may give additional information on the origin of the second, inward-moving component. Outside the expansion, both vdf components have the temperature of the periphery. Towards the expansion axis we see a decrease in temperature of the expanding component, as expected in an expansion. The temperature of the inward-moving component increases, which could be ascribed to collisions with fast, e.g., expanding, particles.

This experimental evidence therefore supports the explanation that the inward-moving atoms come from the periphery of the barrel shock. It suggests the entry of gas from the periphery into the supersonic plasma beam. This entry is possible because the mean free path in the valley is of the order of the radial size of the valley ($Kn \approx 0.5-1$). An atom can move into the expansion, even without noticing, until it collides and is entrained in the expansion. So it only takes place in the rarefied regime. If, on the other hand, the pressure is high and $Kn \ll 1$, the mean free path is much smaller and atoms or molecules cannot enter the expansion.

An example of a consequence of the inflow is shown in Fig. 6, where the axial density profiles of argon atoms and hydrogen atoms are shown in an $Ar-H_2$ plasma. A flow of 50 scc/s argon is used at a current of 40 A. The flow of 8 scc/s of H_2 is injected in two ways: in the cascaded arc and in the vessel. In the first case, H atoms come from the source and in the latter case, the source delivers Ar^+ ions, which react with H_2 forming very efficiently two hydrogen atoms via proton transfer and dissociative recombination.[37] Already in the earliest part of the valley, hydrogen atoms are created at the expansion axis in the case of vessel injection. This clearly proves the fact that hydrogen molecules from the background of the expansion enter into the plasma expansion in the valley of the expansion. A comparison between the atomic hydrogen densities in the case of arc injection and vessel injection may shed some light on the efficiency of the inflow of H_2 into an argon expansion. Already at the end of the shock ($z_M \approx 120$ mm), the densities in both cases have become equal. Downstream, the H density in

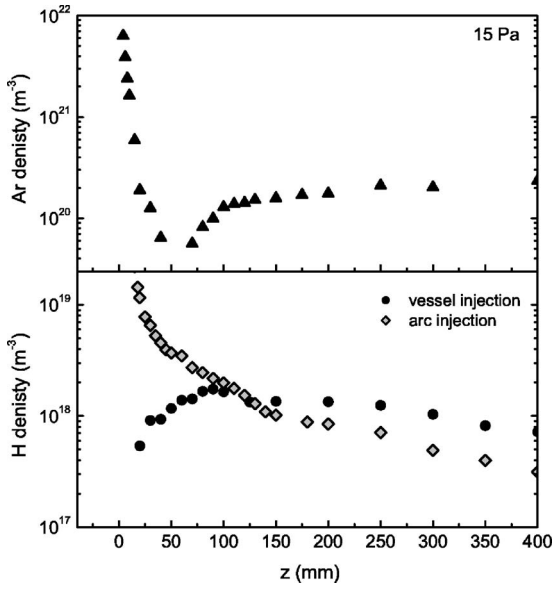

FIG. 6. Axial density profiles of argon atoms (top) and hydrogen atoms (bottom) in an Ar–H_2 plasma. The H_2 gas has been either injected in the arc (◇) or in the vessel (●). The background pressure was 15 Pa, the Ar flow was 50 scc/s, and the H_2 flow was 8 scc/s.

the vessel injection case even remains higher. So H_2 can efficiently enter an argon expansion.

The invading flow may, in a first-order approximation, be estimated by the product of a thermal incident flux through the border of the valley and the probability to be entrained in the supersonic plasma beam,

$$\Phi_{\text{entr}} = \frac{n_b c_b}{4} A_{\text{boun}} \xi_{\text{entr}}, \tag{7}$$

where n_b is the density and c_b is the local sound speed in the periphery of the plasma. A_{boun} is the surface around the valley through which the particles enter and ξ_{entr} is the probability of particle entrainment in the plasma. The boundary around the valley can be estimated by the following formula:

$$A_{\text{boun}} = 2\pi \bar{R}_{\text{vall}} \bar{l}_{\text{vall}} = \pi z_M^2 \xi_{\text{geom}}, \tag{8}$$

in which $\bar{R}_{\text{vall}}$ and $\bar{l}_{\text{vall}}$ are the mean radius and length of the valley. The radius of the valley is slightly smaller than z_M and the length is slightly larger than z_M, leading to Eq. (8). An extra term ξ_{geom} has been added to account for possible geometric deviations of the area of the boundary. Here, we use the first-order estimate of $\xi_{\text{geom}}=1$. The probability of a particle to be entrained in the plasma may be estimated by the product of the probability to reach the axis, ξ_{in}, multiplied with the probability to collide with a supersonic particle in the plasma, ξ_{coll},

$$\xi_{\text{entr}} = \xi_{\text{in}} \xi_{\text{coll}} = e^{-\rho^2}(1 - e^{-\rho^2}) \text{ with } \rho = \frac{\bar{R}_{\text{vall}}}{\lambda_{\text{mfp}}}. \tag{9}$$

This expression is merely a rough, first-order estimate of the entrainment probability, since λ_{mfp} is a function of the radial position in the jet and a more accurate expression should contain an integral form over the radius of the jet. However, using Eq. (8) and using Eq. (5) for z_M in terms of flow and source velocity, the total entering flow determined by Eq. (7) can be related to the total flow of the feed gas in the plasma, Φ_0:

$$\frac{\Phi_{\text{entr}}}{\Phi_0} = 0.81 \xi_{\text{entr}} \xi_{\text{geom}} \sqrt{\frac{A_s}{A_b}\frac{T_s}{T_b}}, \tag{10}$$

where A_s and A_b are the relative mass numbers of particles in the plasma and in the entering flow and T_s and T_b are the temperatures of the source and the periphery of the plasma. Based on this picture and on these assumptions, the inflowing flux can be estimated using Eq. (10). To do so, the probability for entrainment ξ_{entr} needs to be estimated. It has a theoretical maximum value of 1/4, which is approached in the case of a low-pressure hydrogen expansion, $\xi_{\text{entr}} \approx 0.2$. The resulting inflow would be $0.4\Phi_0$. In the case of argon the inflow would be smaller. Using the probability $\xi_{\text{entr}} \approx 0.1$ results in an inflow of $0.2\Phi_0$. As outlined before, this is a first-order approximation, and a more complete description would involve extensive direct simulation Monte Carlo (DSMC) calculations. However, based on the uncertainties in parameters such as $\bar{l}_{\text{vall}}$ (50%) and z_M (25%), and taking into account the remark below Eq. (9), we estimate the outcome of Eq. (10) to be accurate within a factor of 2.

V. SHOCK FORMATION

The inflow of particles into the expansion leads to the deceleration of the particles in the jet. This deceleration is the beginning of the transition from supersonic to subsonic, i.e., the shock, which leads to nonequilibrium vdfs, both in radial and axial directions.[13,14] We will show that in rarefied plasma expansions of argon, but also of hydrogen and nitrogen, the inflow plays an important role in the shock formation.

A. Argon plasma expansion

In Fig. 7 five axial vdfs are shown: one in the supersonic region (a), three in the shock region [(b),(c), and (d)], and one in the subsonic region (e). The axial position is normalized to the Mach disk position z_M resulting in $\hat{z}=z/z_M$. This enables a better comparison for the different gases. In Fig. 7(a), at $\hat{z}=0.35$ the flow is supersonic, as expected, but at $\hat{z}=0.61$, where the density is lowest, the vdf is not Maxwellian anymore. There, the vdf has to be described using a bimodal approximation. There are two flow components that add up to the observed vdf: a fast, cold component and a warm, slow component. The fast, cold component has velocity $2c_0$ and a temperature according to a $\gamma=5/3$ expansion. The warm, slow component has the temperature of the background. This feature becomes more pronounced further on in the shock at $\hat{z}=0.79$. Gradually the supersonic, uncollided component is changed into a decelerated, collided component. At $\hat{z}=1.33$, just after the first shock (there is a slight double-shock structure in the argon expansion and therefore the velocity is still slightly supersonic), the slow component has almost completely taken over. Even further downstream, in the subsonic region, at $\hat{z}=2.33$ only the warm, now subsonic, component resides. This picture of a bimodal approxi-

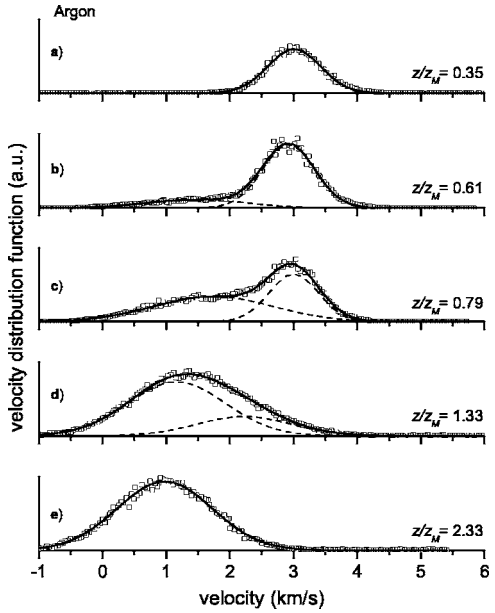

FIG. 7. Axial velocity distribution functions of argon at five axial positions in the plasma jet showing the gradual change from a supersonic to a subsonic distribution. The lines correspond to fits using the bimodal approximation.

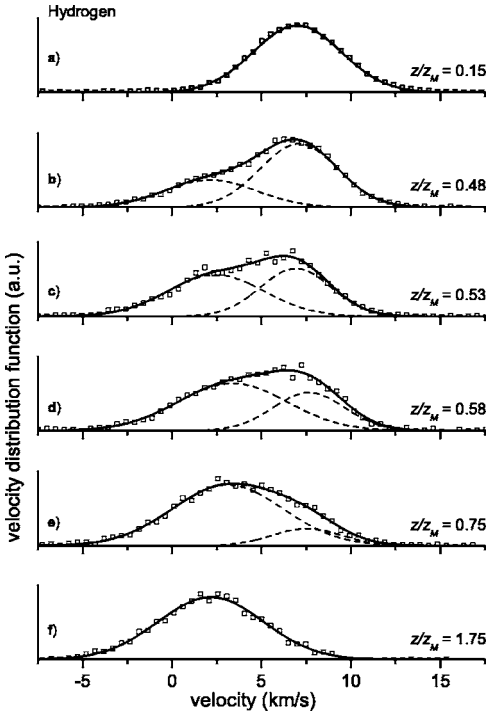

FIG. 8. Axial velocity distribution functions of hydrogen atoms at six axial positions in the plasma jet showing the gradual change from a supersonic to a subsonic distribution. The lines correspond to fits using the bimodal approximation. The background pressure was 20 Pa and the flow was 50 scc/s.

mation, in which freely expanding, cold particles are converted into slow, warm particles, is further supported by the axial profiles of the density ratio, temperature, and velocity of both components, which can be determined from the measured vdfs.[27]

Such a change from a supersonic to a subsonic flow is usually observed in shocks.[13,14] The supersonic flow adapts to the downstream conditions over a finite length in the order of one to several mean free paths. The downstream conditions are matched due to collisions with the downstream particles that may move a distance equal to λ_{mfp} upstream. In the rarefied conditions encountered here, where the mean free path approaches the size of the valley, the shock first takes place over a relatively long distance, e.g., $0.4z_M$ at 20 Pa. And secondly, it may be influenced or even be partly caused by collisions of the supersonic particles with the entering particles that flow into the expansion from the periphery of the expansion. This inflow of particles from the periphery has been discussed in more detail in the previous section.

Another aspect of the bimodal vdf in the shock is the velocity ratio between the two axial components (v_{fast}/v_{slow}). This ratio can give more insight in the exact nature of the collisions that decelerate the freely expanding particles. Especially at the start of the shock, where the freely expanding particles are the majority particles, it may be illustrative for the origin of the collision partners. This axial velocity ratio at the start of the shock is approximately a factor of 2, which is the ratio expected from a collision with a particle with only a transverse velocity component. This is in accordance with the picture of entrained particles influencing the shock formation. As the width of the shock structure is of the order of a mean free path, over this width also a component of the slower subsonic (already shocked) flow is present. This component contains also a small number of particles moving in the opposite direction to the supersonically moving particles in the jet. This effect is only important at the axis and close to the shock front, where it can contribute to the slow velocity component.

B. Hydrogen and nitrogen plasma expansions

The picture of shock formation and entrainment is also encountered in rarefied plasma expansions using other gases such as hydrogen and nitrogen.[15] However, the situation in the molecular plasmas is slightly different from the argon case, since the monitored H and N *atoms* are minority particles and the neutral *molecules* are the main constituent. Furthermore, both hydrogen and nitrogen atoms associate, with high probability, at the vessel walls, which leads to a low partial pressure of hydrogen atoms in the background. Therefore, mainly neutral molecules will flow into and get entrained in the expansion. But since the molecules collide with the atoms (and molecules) in the expansion, the entrainment of peripheral molecules will also be reflected in the H atom vdf. So by observing the H atom vdf we also observe, indirectly, the inward motion of the H_2 molecules.

In Fig. 8, the axial vdfs of H atoms are shown and in Fig. 9 the axial N atom vdfs are shown. In both figures the vdfs are shown at six axial positions in the expansion: the supersonic region (a), the shock (b)–(e), and the subsonic region (f). The behavior in the hydrogen and nitrogen cases is very comparable to the behavior that is observed in the argon expansion. In the shock of the expansion the initially supersonic flow is gradually converted into a subsonic flow by

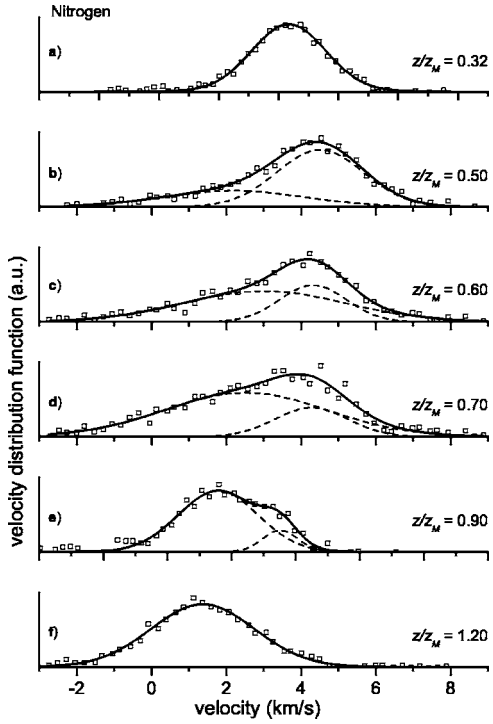

FIG. 9. Axial velocity distribution functions of nitrogen atoms at six axial positions in the plasma jet showing the gradual change from a supersonic to a subsonic distribution. The lines correspond to fits using the bimodal approximation. The background pressure was 20 Pa and the flow was 25 scc/s.

collisions. Part of the collision partners will be entrained molecules from the periphery of the expansion.

In Fig. 10 the H atom axial velocity profile is shown. Both the mean velocity, i.e., the first moment of the distribution, and the individual velocities of the undisturbed and collided components are given. In the expansion region the velocity increases to a velocity of 7400 m/s, which is close to the maximum velocity of H_2 of $2c_0=8000$ m/s, where c_0 is the sound velocity at the source exit. Then, in the shock a bimodal distribution appears. The velocity of the undisturbed component remains at 7400 m/s, whereas the collided component has an initial velocity of 2100 m/s. This component is then accelerated to above 3000 m/s by secondary collisions. At a certain position the collided component is the main component and from thereon the velocity of this component decreases again. The calculation of the velocity ratio of the uncollided to the collided components in the hydrogen (and nitrogen) case is somewhat more complicated, because *molecules* enter the expansion, while the vdf of the *atoms* is measured. Taking the mass ratio of 2 into account leads to a first estimate of the velocity ratio of 3 in a collision with molecules with only transverse velocity. The observed ratio is 3.5 ± 0.5, which overlaps the predicted value. Again this is in accordance with the picture of entraining particles, but it does not exclude particles moving upstream.

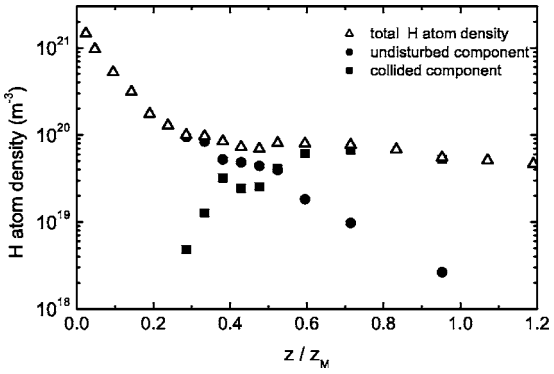

FIG. 11. The H atom density as a function of the normalized axial position in the plasma expansion at a background pressure of 20 Pa. The filled symbols represent the density in the undisturbed and collided components in the bimodal approximation and the open symbols represent the total density.

In Fig. 11 the axial dependence of the H atom density is shown. In the shock, the density does not increase, instead the H atoms diffuse out of the plasma expansion[28] due to the low H atom background density. However, the gradual change from supersonic to subsonic is clearly depicted. The undisturbed, freely expanding component is gradually converted into the collided component. This collided component increases in density until it has completely taken over the flow, indicating the end of the shock.

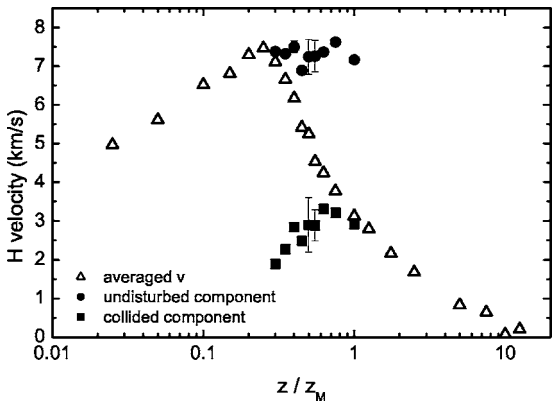

FIG. 10. The axial H atom velocity as a function of the normalized axial position in the plasma expansion at a background pressure of 20 Pa. The filled symbols represent the velocities of the undisturbed and collided components in the bimodal approximation and the open symbols represent the average velocity.

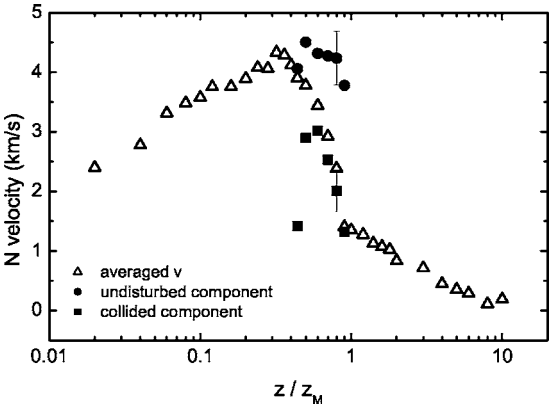

FIG. 12. The axial N atom velocity as a function of the normalized axial position at a background pressure of 20 Pa. The filled symbols represent the velocities of the undisturbed and collided components in the bimodal approximation and the open symbols represent the average velocity.

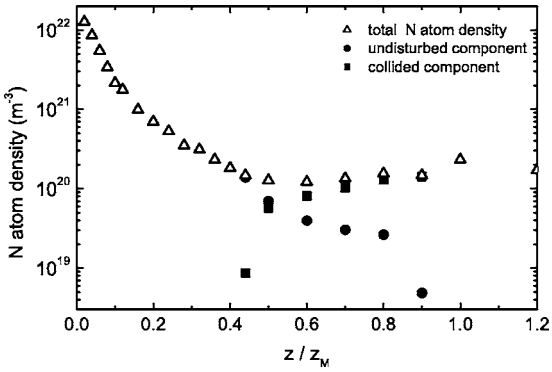

FIG. 13. The N atom density as a function of the normalized axial position at a background pressure of 20 Pa. The filled symbols represent the density in the undisturbed and collided components in the bimodal approximation and the open symbols represent the total density.

The axial dependencies of the velocity and density of a nitrogen plasma expansion are shown in Figs. 12 and 13. The same view holds as in the hydrogen case. The plasma flow expands and is accelerated to a velocity of around 4400 m/s, which is close to the maximum velocity of nitrogen molecules. Then this fast component is decelerated by collisions with particles that may come from the periphery and a second flow component arises. Moving downstream, this second component gains density on account of the undisturbed component until the end of the shock, where it has completely taken over. The observed velocity ratio of 3.1 is very close to the earlier given value of 3.

To visualize the similarity between the hydrogen and nitrogen expansion the velocity profiles have been normalized, as depicted in Fig. 14. The velocity is normalized to the sound velocity at the source exit, c_0, and the axial position to the Mach disk position. The velocity profiles are very similar in the subsonic and supersonic expansion regimes. In the supersonic expansion region, both velocities are accelerated from sonic speed at the exit of the source towards twice this velocity, which is the predicted maximum reachable velocity, see Eq. (4). However, this velocity is not reached for both gases. Apparently, the shock is formed a little too close to the source for the frozen regime (velocity at maximum value) to set in. In the shock region, the scaled velocity profiles differ slightly. Nitrogen atoms expand a little further and the velocity drops more quickly. This is a consequence of the chosen scaling. Inside the shock wave a different scaling should be applied.[15] The applied scaling does give a very acceptable description of the velocity in the expansion, which is independent of gas, source temperature, or flow.

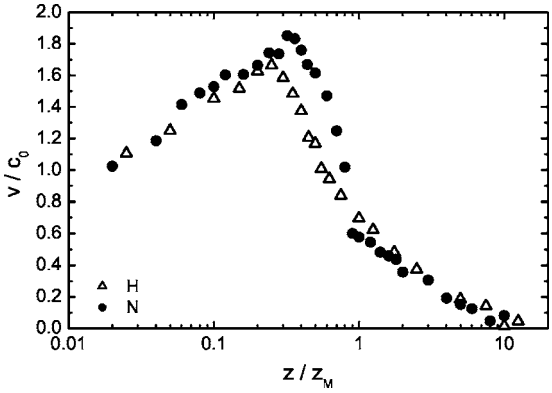

FIG. 14. Normalized velocity as a function of the normalized axial position for both H atoms in a hydrogen plasma expansion and N atoms in a nitrogen plasma expansion.

VI. CONCLUSIONS

We have presented measured velocity distributions in rarefied plasma expansions of argon, hydrogen, and nitrogen. The vdfs in the valley of the expansion show a bimodal character that may be caused by the inflow of particles from the periphery of the plasma into the primary beam. Since the inflow could be considerable compared to the total flow from the source, it may significantly enhance the admixture of precursor gases for high-rate deposition and surface modification. Bimodal distributions are, furthermore, encountered in the shock of the expansions, where they show in great detail the change from a supersonic to a subsonic flow.

ACKNOWLEDGMENTS

This work is part of the research program of the Dutch Foundation for Fundamental Research on Matter (FOM). The work is also supported by the Euratom Foundation. We greatly appreciate the skillful technical assistance of M. J. F. van de Sande, J. F. C. Jansen, A. B. M. Hüsken, and H. M. M. de Jong.

[1] *Beams and Jets in Astrophysics*, edited by P. A. Hughes (Cambridge University Press, 1991).
[2] J. C. Angus and C. C. Hayman, Science **241**, 913 (1988).
[3] A. Lebéhot and R. Campargue, Phys. Plasmas **3**, 2502 (1996).
[4] M. C. M. van de Sanden, R. J. Severens, W. M. M. Kessels, R. F. G. Meulenbroeks, and D. C. Schram, J. Appl. Phys. **84**, 2426 (1998).
[5] S. Sriraman, S. Agarwal, E. S. Aydil, and D. Maroudas, Nature (London) **418**, 62 (2002).
[6] E. T. Curran and S. N. B. Murthy, *Scramjet Propulsion*, Progress in Astronautics and Aeronautics Series Vol. 189 (American Institute of Aeronautics and Astronautics, 2001).
[7] E. J. Gutmark, K. C. Schadow, and K. H. Yu, Annu. Rev. Fluid Mech. **27**, 375 (1995).
[8] J. Benedikt, Ph.D. thesis, Eindhoven University of Technology, 2004, available on-line at http://alexandria.tue.nl/extra2/200412861.pdf
[9] J. W. A. M. Gielen, P. R. M. Kleuskens, M. C. M. van de Sanden, L. J. van IJzendoorn, D. C. Schram, E. H. A. Dekempeneer, and J. Meneve, J. Appl. Phys. **80**, 5986 (1996).
[10] A. de Graaf, Ph.D. thesis, Eindhoven University of Technology, 2000, available on-line at http://alexandria.tue.nl/extra2/200011593.pdf
[11] J. P. M. Hoefnagels, Y. Barrell, W. M. M. Kessels, and M. C. M. van de Sanden, J. Appl. Phys. **96**, 4094 (2004).
[12] J. R. Abelson, Appl. Phys. A: Solids Surf. **56**, 493 (1993).
[13] H. M. Mott-Smith, Phys. Rev. **82**, 885 (1951).
[14] G. Pham-Van-Diep, D. A. Erwin, and E. P. Muntz, Science **245**, 624 (1989).
[15] S. Mazouffre, P. Vankan, R. Engeln, and D. C. Schram, Phys. Rev. E **64**, 066405 (2001).
[16] H. Ashkenas and F. S. Sherman, in *Proceedings of the Fourth International Symposium on Rarefied Gas Dynamics*, edited by J. H. de Leeuw (Academic, New York, 1966), Vol. 2, p. 84.
[17] R. Campargue, J. Chem. Phys. **52**, 1795 (1970).
[18] H. C. W. Beijerink, R. J. F. van Gerwen, E. R. T. Kerstel, J. F. M. Martens, E. J. W. van Vliembergen, M. R. T. Smits, and G. H. Kaashoek, Chem. Phys. **96**, 153 (1984).
[19] M. C. M. van de Sanden, J. M. de Regt, and D. C. Schram, Plasma Sources Sci. Technol. **3**, 501 (1994).

[20]D. C. Schram, S. Mazouffre, R. Engeln, and M. C. M. van de Sanden, *Atomic and Molecular Beams*, edited by R. Campargue (Springer, New York, 2001), p. 209.
[21]The total pressure corresponds to the sum of the static pressure nkT and the dynamic pressure $\frac{1}{2}nmv^2$.
[22]G. M. Janssen, Ph.D. thesis, Eindhoven University of Technology, 2000, available on-line at http://alexandria.tue.nl/extra2/200013063.pdf
[23]D. R. Miller, *Atomic and Molecular Beam Methods* (Oxford University, New York, 1988), Chap. 2.
[24]L. D. Landau and E. M. Lifshitz, *Fluid Mechanics* (Pergamon, London, 1959).
[25]P. Vankan, D. C. Schram, and R. Engeln, J. Chem. Phys. **121**, 9876 (2004).
[26]W. S. Young, Phys. Fluids **18**, 1421 (1975).
[27]R. Engeln, S. Mazouffre, P. Vankan, D. C. Schram, and N. Sadeghi, Plasma Sources Sci. Technol. **10**, 595 (2001).
[28]S. Mazouffre, P. Vankan, R. Engeln, and D. C. Schram, Phys. Plasmas **8**, 3824 (2001).
[29]S. Mazouffre, I. Bakker, P. Vankan, R. Engeln, and D. C. Schram, Plasma Sources Sci. Technol. **11**, 439 (2002).
[30]P. Vankan, R. Engeln, and D. C. Schram, Appl. Phys. Lett. **86**, 101501 (2005).
[31]S. Mazouffre, P. Vankan, W. M. M. Kessels, R. Engeln, M. C. M. van de Sanden, and D. C. Schram, IEEE Trans. Plasma Sci. **30**, 146 (2002).
[32]M. C. M. van de Sanden, J. M. de Regt, and D. C. Schram, Phys. Rev. E **47**, 2792 (1993).
[33]M. J. de Graaf, R. Severens, R. P. Dahiya, M. C. M. van de Sanden, and D. C. Schram, Phys. Rev. E **48**, 2098 (1993).
[34]S. Brussaard, Ph.D. thesis, Eindhoven University of Technology, 1999, available on-line at http://alexandria.tue.nl/extra2/9900312.pdf
[35]M. G. H. Boogaarts, S. Mazouffre, G. J. Brinkman, H. W. P. van der Heijden, P. Vankan, J. A. M. van der Mullen, D. C. Schram, and H. F. Döbele, Rev. Sci. Instrum. **73**, 73 (2002).
[36]P. Vankan, S. B. S. Heil, S. Mazouffre, R. Engeln, D. C. Schram, and H. F. Döbele, Rev. Sci. Instrum. **75**, 996 (2004).
[37]S. Mazouffre, M. G. H. Boogaarts, I. S. J. Bakker, P. Vankan, R. Engeln, and D. C. Schram, Phys. Rev. E **64**, 016411 (2001).